GEOPHYSICAL RESEARCH LETTERS, VOL. 29, NO. 20, 2000, doi:10.1029/2002GL015994, 2002

Ribbon spacing in Venusian tessera: Implications for layer thickness and thermal state

Rebecca R. Ghent
Center for Earth and Planetary Studies, Smithsonian Institution, Washington, DC, USA

Ileana M. Tibuleac
Weston Geophysical Corporation, Lexington, MA, USA

Received 29 July 2002; revised 17 September 2002; accepted 19 September 2002; published 31 October 2002.

[1] We report on measurements of characteristic extensional wavelength represented by ribbons in Venusian tessera terrain. Fourier power spectra for ribbons in 35 areas from 9 geographic regions show dominant wavelengths of 2 to 6 km. We used these values to estimate mechanical layer thickness during ribbon formation at 0.6 to 2.9 km. Because ribbons accommodate extension of a single strong layer overlying a ductile substrate, we conclude that the base of this mechanical layer corresponded to the local brittle-ductile transition (BDT) during ribbon formation. Maintaining a BDT at <3 km depth for a significant length of time requires a locally hot environment, as over a plume impinging on thin lithosphere. These results indicate that locally hot conditions prevailed at widely distinct locations in the past. *INDEX TERMS:* 6295 Planetology: Solar System Objects: Venus; 8015 Structural Geology: Local crustal structure; 8010 Structural Geology: Fractures and faults; 5475 Planetology: Solid Surface Planets: Tectonics (8149); 8159 Tectonophysics: Evolution of the Earth: Rheology—crust and lithosphere. **Citation:** Ghent, R. R., and I. M. Tibuleac, Ribbon spacing in Venusian tessera: Implications for layer thickness and thermal state, *Geophys. Res. Lett.*, *29*(20), 2000, doi:10.1029/2002GL015994, 2002.

1. Introduction

[2] The origins, evolutionary history, and spatial extent of Venusian tessera terrain have been deliberated since Magellan synthetic aperture radar (SAR) images [*Saunders et al.*, 1992] provided high-resolution views of Venus' surface [e.g., *Bindschadler et al.*, 1992a, 1992b; *Gilmore et al.*, 1997, 1998; *Hansen and Willis*, 1996, 1998; *Ivanov and Head*, 1996; *Ghent and Hansen*, 1999; *Hansen et al.*, 2000]. Tessera terrain was initially defined as any surface showing at least two intersecting lineament sets [*Barsukov et al.*, 1986; *Basilevsky et al.*, 1986]. *Hansen and Willis* [1996] further classified tessera into several types based on the structural patterns represented. One such type is characterized by "ribbons" [*Hansen and Willis*, 1996, 1998], or long, narrow, shallow, flat-floored, steep troughs (Figure 1). Ribbons form a delicate, penetrative, spatially periodic fabric over four of Venus' five crustal plateaus and many large tessera inliers within the plains. In a detailed structural analysis, *Hansen and Willis* [1998] explored possible mechanisms for ribbon formation, and documented strong evidence for ribbons as extensional features. Those workers proposed that ribbons accommodate extension in a thin brittle surface layer above a ductile substrate, as might occur over a large plume impinging on thin lithosphere. *Hansen and Willis* [1998] also interpreted ribbons as the oldest preserved structures in each occurrence of crustal plateau tessera. *Gilmore et al.* [1998] suggested that ribbons instead represent a late extensional fabric that overprints earlier folds. *Ghent and Hansen* [1999] addressed the relative timing issue by measuring ribbon spacing in Ovda Regio, and used established spacing-to-layer thickness relationships to estimate a maximum mechanical layer thickness in that region during ribbon formation of ~1–2 km. Those workers observed that ribbons represent the only spatially periodic extensional structures in the region. The absence of additional extensional fabrics with distinct wavelengths argued against the existence of multiple strong layers in the lithosphere, as might result from large-scale compositional layering or mechanical disruption of the surface layer. This led Ghent and Hansen to propose that during ribbon formation, the base of the extending layer was actually the local thermally-defined brittle-ductile transition (BDT). This led to a three-phase strain history for Ovda Regio characterized by early dominant, widespread, and pervasive extension (expressed as ribbons), consistent with the plume model for crustal plateau origin proposed by *Hansen and Willis* [1998] and *Phillips and Hansen* [1998].

[3] In this work, we also treated the base of the ribbon-forming layer as synonymous with the local, transient, thermally-defined BDT (though we did not further address the relative timing of ribbons and other structures). We investigated geographic variations in mechanical layer thickness during ribbon formation by computing the dominant structural wavelength(s) represented in each of 35 ribbon-bearing areas in crustal plateaus and tessera inliers using Fourier power spectra. We took this spacing to result from an extensional layer instability, and we applied theoretical wavelength-to-layer thickness ratios to estimate surface layer thickness during ribbon formation in each region. Though other measurements of shear-fracture ribbon spacing in limited regions have been performed [e.g., *Hansen and Willis*, 1998; *Ghent and Hansen*, 1999], the current work represents the first attempt to quantify their characteristic wavelengths using an objective and reproducible method. Further, our current work investigates for the first time the global geographic variation in layer thickness during ribbon formation and the resulting rheological implications. If the effective mechanical layer thickness during

Copyright 2002 by the American Geophysical Union.
0094-8276/02/2002GL015994$05.00

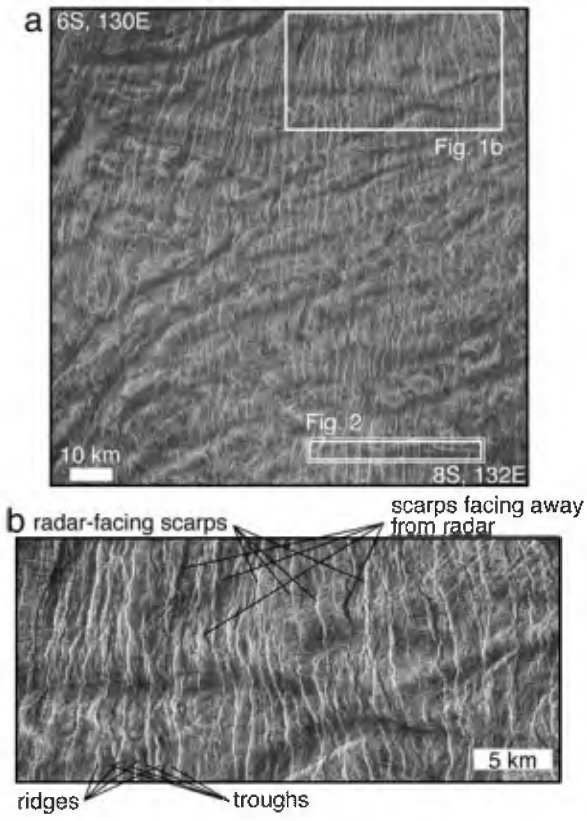

Figure 1. (a) Magellan SAR image taken from Thetis Regio showing the continuous, delicate ribbon fabric (illuminated from the left). Double box shows location of transect in Figure 2. (b) Detail of region marked with single box in (a). Image shows detailed shear-fracture ribbon morphology.

ribbon formation was in fact thermally mediated, then constraining its value in a given area yields information about the local thermal regime at that time. This in turn provides valuable input into the ongoing discussion of competing geodynamic models for Venus.

2. Method

[4] In Magellan SAR images, ribbons oriented nearly normal to the incident radar appear as sets of alternating bright and dark lineaments separated by broader surfaces with intermediate tones (Figure 1). Trough-bounding scarps facing the radar appear as bright lineaments, ridges and trough floors appear as wide lineaments or surfaces of intermediate tones, and trough-bounding scarps facing away from the radar appear as dark lineaments. Trough walls commonly show multiple bright or dark lineaments. Plotting grayscale values vs. position along a given transect perpendicular to ribbon trends yields a spatial "signal;" an example is shown in Figure 2.

[5] Ribbons have two end-member morphologies: "tensile-fracture" and "shear-fracture" ribbons, named for their respective fracture modes [*Hansen and Willis*, 1998]. Tensile-fracture ribbons are tensile opening fractures with matching walls and V-shaped terminations and are dominant in western Fortuna Tessera but rare in other crustal plateaus. More common are shear-fracture ribbons, which are essentially long, narrow, shallow graben bounded by normal faults. For shear-fracture ribbons, the relevant spacing is measured between corresponding points on adjacent structures (e.g., corresponding trough walls). In a brightness spatial series, this is the distance between successive brightness maxima or minima. This yields a distance equal to the incipient failure wavelength plus subsequent extension; the resulting uncertainty is unavoidable for shear-fracture ribbons without an independent estimate of finite extension [*Ghent and Hansen*, 1999]. Estimating the characteristic extensional wavelength in this way results in upper bounds on estimates of layer thickness during ribbon formation.

[6] We computed Fourier power spectra for 35 examples of characteristic shear-fracture ribbon terrain from 9 geographic regions. The chief criterion for area selection was length of potential transects with well-developed, undisturbed ribbons. We avoided areas showing ribbon reactivation, lava flooding, or other disruption. Each study area was bounded by a box 1024 pixels (76.8 km) long by 100 pixels (7.5 km) wide, oriented with its long axis perpendicular to ribbon trends (Figure 1). Each box included 15–25 complete ribbon structures. We averaged brightness values for five equally spaced one-pixel-wide transects normal to ribbon trends from each box to reduce short-wavelength noise. Post-transform stacking yielded similar results. Full-resolution Magellan SAR data has a resolution of 13.33 pixels per kilometer, so the spatial Nyquist frequency is 6.67 km^{-1}. We computed the averaged Fourier power spectral density using a moving 512 sample Hanning window [e.g., *Ambardar*, 1995] overlapping by 50%. The dominant ribbon spacing(s) for each study area was obtained from the wavelength(s) corresponding to the largest spectral peak(s) in the relevant band. The related uncertainty was controlled by the smoothing window bandwidth, and scaled with wavelength. We benchmarked our method against manual measurements of spacing for morphologically simple ribbons. We also made spectral estimations of ribbon spacing using Walsh functions for comparison with the Fourier power spectral results [e.g., *Walsh*, 1923; *Harmuth*, 1972; *Beauchamp*, 1975]; the results showed close agreement with those presented here (see *Ghent* [2002] for details).

3. Results

[7] The results are summarized in Table 1. All of the calculated dominant wavelengths fell within a range of

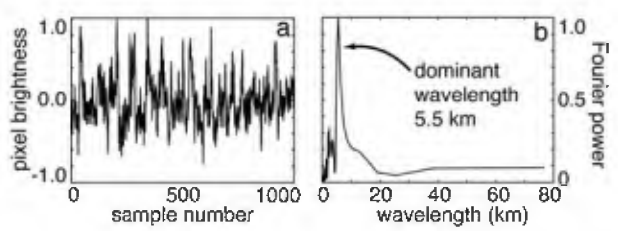

Figure 2. (a) Pre-transform averaged spatial series for 5 transects from study area shown in Figure 1 (double box); brightness values are normalized (white: 1, black: −1). (b) Normalized Fourier power spectrum for signal in (a). This spectrum has a single dominant peak at 5.5 km.

Table 1. Summary of Spacing Results

Region	Transect lat/lon (E)/ trend	$\lambda_1 \pm \delta^a$ (km)	$\lambda_2 \pm \delta^a$ (km)	h (km)[b]
Alpha	−22.5; 2.3; 025	4.8 ± 1.1		1.5–2.0
Regio	−22.9; 5.1; 315	4.9 ± 1.2		1.5–2.0
	−27.0; 0.5; 055	*2.4 ± 0.3*	4.8 ± 1.1	1.5–1.9
	−27.6; 3.2; 040	6.0 ± 2.0		2.0–2.7
	−19.5; 5.5; 070	3.8 ± 0.7		1.1–1.5
Ananke Tessera	59.7; 124.9; 025	4.2 ± 0.9		1.3–1.7
Gbadu	1.3; 39.6; 040	3.2 ± 0.5		0.9–1.2
Tessera	1.1; 44.9; 090	*5.0 ± 1.2*	2.5 ± 0.3	1.6–2.1
Manatum Tessera	−3.9; 49.2; 040	3.4 ± 0.6		1.0–1.3
Eastern/	−5.6; 99.5; 025	5.1 ± 1.3	3.2 ± 0.5	1.6–2.1
Central	−2.0; 83.5; 045	*3.2 ± 0.5*	2.3 ± 0.3	0.9–1.2
Ovda	−6.6; 74.6; 335	3.7 ± 0.7		1.1–1.5
Regio	−9.2; 79.3; 090	4.2 ± 0.9	2.7 ± 0.4	1.3–1.7
	−8.8; 80.4; 090	2.7 ± 0.4		0.8–1.0
Western	4.8; 65.1; 065	3.9 ± 0.8	*2.5 ± 0.3*	1.2–1.6
Ovda	4.3; 67.4; 280	4.9 ± 0.2		1.3–1.7
Regio	4.4; 68.4; 290	4.8 ± 1.2		1.5–2.0
	−3.6; 54.4; 075	4.0 ± 0.9	*2.1 ± 0.2*	1.2–1.6
	−8.4; 64.9; 065	5.4 ± 1.5		1.7–2.3
	−11.5; 54.4; 050	3.3 ± 0.5	2.1 ± 0.2	1.0–1.3
	11.7; 59.5; 285	5.0 ± 1.3		1.6–2.1
Tellus	29.7; 76.9; 310	5.2 ± 1.4		1.7–2.2
Tessera	32.6; 76.8; 320	2.4 ± 0.3	*3.3 ± 0.7*	1.0–1.3
	33.2; 79.4; 320	2.4 ± 0.3	*4.6 ± 1.2*	1.5–1.9
Tethus	67.3; 108.5; 325	2.3 ± 0.2		0.6–0.8
Regio	66.7; 123.3; 345	3.6 ± 0.7		1.1 –1.4
Thetis	7.7; 127.4; 055	4.0 ± 0.8	6.7 ± 2.1	2.2–2.9
Regio	4.4; 120.8; 055	2.0 ± 0.2	*3.6 ± 0.6*	1.1 –1.4
	4.7; 134.9; 065	4.7 ± 1.1	3.6 ± 0.6	1.5–1.9
	1.6; 132.0; 035	3.7 ± 0.7		1.1 –1.5
	−5.3; 120.9; 035	5.6 ± 1.6	3.6 ± 0.7	1.8–2.4
	−3.1; 131.5; 293	3.1 ± 0.5		0.9–1.2
	−6.0; 134.6; 090	4.9 ± 1.3		1.6–2.1
	−7.8; 131.2; 090	5.4 ± 1.5	2.3 ± 0.3	1.7–2.3
	−8.1; 131.1; 090	4.8 ± 1.2		1.5–2.0

[a] λ_1, λ_2:wavelength of primary and secondary peaks, respectively.
[b] h: layer thickness; italicized values reflect non-ribbon features.

2–6 km. Twenty of the 35 spectra showed single strong peaks within this range (e.g., Figure 2b); the other 15 showed two or more significant peaks. For all but five of these cases, the two major peaks were of approximately equal amplitude; for unequal peaks, the larger exceeded the smaller by at most a factor of 1.6. In seven of the 15 polymodal cases, both the primary and secondary peaks reflected ribbon wavelengths. This results when imaged ribbons accommodate varying degrees of extension, or where adjacent trough walls merge, leading to a variation in trough width along the transect. Shear-fracture ribbon trough walls commonly show multiple lineaments, which also give rise to multiple peaks. For the other polymodal spectra, we distinguished the peak corresponding to the ribbon wavelength by examining SAR images. In several of these cases, the shorter of the two was the ribbon wavelength and the longer wavelength peak reflected other features, such as widely spaced ridges intersecting a given transect at an angle.

4. Discussion

[8] A large body of work details theoretical relationships between the thickness of an extending layer embedded in or overlying a less competent matrix and the resulting structural wavelength [e.g., *Ramberg*, 1955; *Smith*, 1975, 1977]. *Fletcher and Hallet* [1983] performed a perturbation analysis using a model lithosphere with a plastic layer over a substrate with depth-dependent viscosity. They identified the dominant wavelength as 3.4 to 4 times the layer thickness for a range of conditions. *Zuber et al.* [1986] used a similar analysis to examine dominant extensional wavelengths in a stratified lithosphere consisting of a strong upper crust, a weak lower crust, and a strong upper mantle. They predicted two wavelengths of extension, with the short wavelength ranging from 2.78 to 2.96 times the upper strong layer thickness. Based on the analytical results summarized above, we used wavelength-to-layer thickness ratios of 3–4 to infer layer thickness during ribbon formation, and arrived at layer thickness estimates of 0.6 to 2.9 km (Table 1). Taking the spacing values reported in Table 1 to represent the fundamental extensional wavelength yields an upper bound on layer thickness during ribbon formation, because we lack an independent estimate of the amount of finite extension accommodated during or after ribbon formation. With this caveat, we calculated layer thicknesses using the upper bound on ribbon spacing in each case, in order to obtain maximum estimates. We observed two striking aspects of these results.

1. Layer thickness estimates for the 9 geographic regions showed a large degree of overlap; in fact, they were essentially indistinguishable (Figure 3). This lends support to the notion that discrete occurrences of ribbon-bearing tessera terrain formed by similar processes, though not necessarily at the same time [*Phillips and Hansen*, 1994, 1998]. In addition, tessera inliers in the plains commonly occur as discontinuous pieces with similar structural patterns to extant crustal plateaus and in some cases show circular planforms; thus tessera inliers may represent crustal plateaus in various stages of degradation [*Campbell and Rogers*, 1994; *Phillips and Hansen*, 1994, 1998; *Zimbelman, J.R.*, Geologic map of the Kawelu Planitia quadrangle (V16), Venus, submitted to the USGS, 2002.].

2. All of the ribbon-bearing regions examined in this study showed dominant wavelengths within a narrow range, reflecting a similarly narrow range in surface layer thickness during ribbon formation. The absence of additional periodic extensional fabrics with distinct characteristic wavelengths is inconsistent with compositional or other mechanical layering at the plateau scale. For instance, a strong-weak-strong rheology would lead to two distinct extensional wavelengths expressed as spatially periodic tectonic structures on two scales, as in the Basin and Range province on Earth [e.g., *Zuber et al.*, 1986]. At the plateau scale, then, it seems that a thermal mechanism is the simplest way to produce a uniform strong-over-weak rheology. Thus, our results suggest that in at least 9 distinct regions, conditions

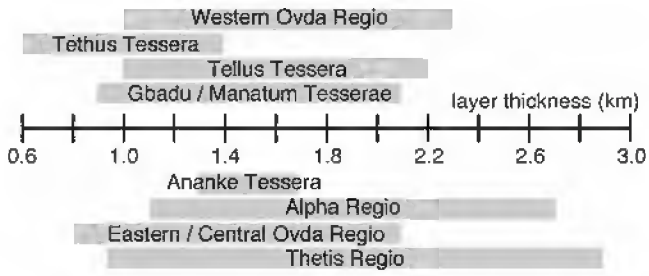

Figure 3. Diagram showing ranges of surface layer thickness during ribbon formation for each of the geographic regions, based on ribbon spacing reported in Table 1.

were sufficiently hot at some time to achieve a local BDT within 3 km of the surface for a significant length of time (e.g., 1 Myr). This result supports the model of crustal plateau origin in which a large mantle plume impinging on thin lithosphere during a former period of mobile-lid tectonics could thin the lithosphere significantly, leading to large degrees of partial melting and local intrusive and volcanic activity [*Hansen and Willis*, 1998; *Phillips and Hansen*, 1998; *Hansen et al.*, 2000]. Theoretical lithospheric yield strength profiles under such conditions reflect a shallow BDT over the hypothetical plume. Indeed, a sufficient thermal flux into thin lithosphere could induce creep all the way to the surface. Waning of the plume would cause the local BDT to deepen, producing an increasingly strong and thick mechanical surface layer capable of recording tectonic structures. Using a 1-D transient halfspace cooling model, *Phillips and Hansen* [1998] and *Hansen et al.* [2000] showed that preserving a sufficiently shallow BDT for a significant length of time requires an elevated surface temperature in addition to thermal input by a plume. Independently, atmospheric work by *Bullock and Grinspoon* [2001] and *Phillips et al.* [2001] raised the possibility that Venus may have experienced periods of elevated surface temperature due to magmatic outgassing during formation of the volcanic plains. It should be noted that though *Bullock and Grinspoon's* thermal history assumed a catastrophic resurfacing event, the model of *Phillips et al.* incorporated an extended period of plains emplacement at a much slower rate and resulted in surface temperatures approaching 1000K for a long time prior to the global transition to stagnant lid convection and thick lithosphere. Globally elevated surface temperature and thin lithosphere persisting for long periods would favor temporally punctuated crustal plateau formation by individual plumes, leading to the current distribution of preserved and degraded plateaus.

5. Conclusion

[9] We conclude that characteristic extensional wavelengths represented by ribbon terrain, wherever it occurs, indicate a locally thin mechanical surface layer. If this layer was thermally controlled, then each instance of ribbon-bearing tessera indicates similarly hot conditions, as in the case of individual plumes impinging on thin lithosphere. Furthermore, because tessera inliers may represent crustal plateaus in various stages of degradation, we expect that this type of local heating event occurred many times in Venus' past, resulting in formation of many crustal plateaus, only a few of which are currently preserved. Because an elevated surface temperature was likely required to maintain the necessarily thin mechanical layer, the widespread distribution of ribbon terrain might thus help constrain the nature of past thermal atmosphere-interior coupling, as outlined by *Phillips et al.* [2001].

[10] **Acknowledgments.** We thank C.D. Brown and an anonymous reviewer for comments that greatly improved the manuscript. This work was supported in part by a Texas Space Grant consortium fellowship to R.R. Ghent.

References

Ambardar, A., *Analog and Digital Signal Processing*, PWS Publishing Company, Boston, MA, 1995.

Barsukov, V. L., The geology and geomorphology of the Venus surface as revealed by the radar images obtained by Veneras 15 and 16, *J. Geophys. Res.*, *91*, D378–D398, 1986.

Basilevsky, A. T., A. A. Pronin, L. B. Ronca, V. P. Kryuchkov, A. L. Sukhanov, and M. S. Markov, Styles of tectonic deformation on Venus: Analysis of Venera 15 and 16 data, *J. Geophys. Res.*, *91*, D399–D411, 1986.

Beauchamp, K. G., *Walsh functions and their applications*, Academic Press, London, 1975.

Bindschadler, D. L., G. Schubert, and W. M. Kaula, Coldspots and hotspots: Global tectonics and mantle dynamics of Venus, *J. Geophys. Res.*, *97*, 13,495–13,532, 1992a.

Bindschadler, D. L., A. deCharon, K. K. Beratan, S. E. Smrekar, and J. W. Head, Magellan observations of Alpha Regio: Implications for formation of complex ridged terrains on Venus, *J. Geophys. Res.*, *97*, 13,563–13,577, 1992b.

Bullock, M. A., and D. H. Grinspoon, The recent evolution of climate on Venus, *Icarus*, *150*, 19–37, 2001.

Campbell, B. A., and P. G. Rogers, Bell, Regio, Venus: Integration of remote sensing data and terrestrail analogs for geologic analysis, *J. Geophys. Res.*, *99*, 21,135–21,171, 1994.

Fletcher, R. C., and B. Hallet, Unstable extension of the lithosphere: A mechanical model for Basin-and-Range structures, *J. Geophys. Res.*, *88*, 7457–7466, 1983.

Ghent, R. R., An analysis of tectonic structures in Venusian crustal plateaus: Structure, kinematics, and numerical modeling, Ph.D. thesis, Southern Methodist University, Dallas, TX, 2002.

Ghent, R. R., and V. L. Hansen, Structural and kinematic analysis of eastern Ovda Regio Venus: Implications for crustal plateau formation, *Icarus*, *139*, 116–136, 1999.

Gilmore, M. S., M. A. Ivanov, J. W. Head, and A. T. Basilevsky, Duration of tessera deformation on Venus, *J. Geophys. Res.*, *102*, 13,357–13,368, 1997.

Gilmore, M. S., G. C. Collins, M. A. Ivanov, L. Marinangeli, and J. W. Head, Style and sequence of extensional structures in tessera terrain Venus, *J. Geophys. Res.*, *102*, 13,357–13,368, 1998.

Hansen, V. L., and J. J. Willis, Structural analysis of a sampling of tesserae: Implications for Venus geodynamics, *Icarus*, *123*, 296–312, 1996.

Hansen, V. L., and J. J. Willis, Ribbon terrain formation, southwestern Fortuna Tessera, Venus: Implications for lithosphere evolution, Icarus, *132*, 321–343, 1998.

Hansen, V. L., R .J. Phillips, J. J. Willis, and R. R. Ghent, Structures in tessera terrain: Issues and answers, *J. Geophys. Res.*, *105*, 4135–4152, 2000.

Harmuth, H. F., *Transmission of Information by Orthogonal Functions*, Springer-Verlag, Berlin, 1972.

Ivanov, M. A., and J. W. Head, Tessera terrain on Venus: A survey of the global distribution, characteristics, and relation to surrounding units from Magellan data, *J. Geophys. Res.*, *101*, 14,861–14,908, 1996.

Phillips, R. J., and V. L. Hansen, Tectonic and magmatic evolution of Venus, *Ann. Rev. Earth Planet. Sci.*, *22*, 597–654, 1994.

Phillips, R. J., and V. L. Hansen, Geological evolution of Venus: A geodynamical and magmatic framework, *Science*, *279*, 1492–1497, 1998.

Phillips, R. J., M. A. Bullock, and S. A. Hauck, II, Climate and interior coupled evolution on Venus, *Geophys. Res. Lett.*, *28*, 1779–1782, 2001.

Ramberg, H., Natural and experimental boudinage and pinch-and-swell structures, *J. Geol.*, *63*, 512–526, 1955.

Saunders, S., J. Spear, P. C. Allin, R. S. Austin, A. L. Berman, R. C. Chandlee, J. Clark, A. V. DeCharon, E. M. DeJong, D. G. Griffith, J. M. Gunn, S. Hensley, W. T. K. Johnson, C. E. Kirby, D. S. Leung, D. T. Lyons, G. A. Michaels, J. Miller, R. B. Morris, A. D. Morrison, R. G. Piereson, J. F. Scott, S. J. Shaffer, J. P. Slonski, E. R. Stofan, T. W. Thompson, and S. D. Wall, Magellan Mission Summary, *J. Geophys. Res.*, *97*, 13,067–13,090, 1992.

Smith, R. B., Unified theory of the onset of folding, boudinage, and mullion structure, *GSA Bull.*, *86*, 1601–1609, 1975.

Smith, R. B., Formation of folds, boudinage, and mullions in non-Newtonian materials, *GSA Bull.*, *88*, 312–320, 1977.

Walsh, J. L., A closed set of orthogonal functions, *Ann. J. Mathematics*, *55*, 5–24, 1923.

Zuber, M. T., E. M. Parmentier, and R. C. Fletcher, Extension of continental lithosphere: A model for two scales of Basin and Range deformation, *J. Geophys. Res.*, *91*, 4826–4838, 1986.

R. Ghent, Center for Earth and Planetary Studies, Smithsonian Institution, P.O. Box 37012, Washington, D. C., 20013-7012, USA. (ghentr@nasm.si.edu)

I. M. Tibuleac, Weston Geophysical Corporation, 57 Bedford Street, Suite 102, Lexington, MA 02420, USA.